Multi-Site Wireless Channel Charting Through Latent Space Alignment

Yamil Vindas, Maxime Guillaud

Multi-Site Wireless Channel Charting Through Latent Space Alignment

Yamil Vindas, Maxime Guillaud
Inria, MARACAS Team & CITI Laboratory, Lyon, France
email: {yamil.vindas-yassine@inria.fr, maxime.m.guillaud@ieee.org}

***Abstract*—Wireless channel charting is a self-supervised machine learning approach designed to capture and leverage the statistical properties of wireless propagation. By applying dimensionality reduction to channel state information, channel charting establishes a low-dimensional representation of the channel state, which is akin to a pseudo-location of the users within the propagation environment. Conversely to multipoint channel charting, which considers efficient ways of fusing the features acquired by multiple access points, we introduce in this work the multi-site channel charting problem whereby multiple base stations generate their own channel charts, while their coverage areas partially overlap. We introduce several methods to align the latent spaces at each base station into a common latent space, effectively performing the fusion of multiple channel charts. We benchmark the proposed approaches and compare their performance in terms of the classical dimensionality reduction metrics using measured data, as well as their degree of distributedness.**

I. Introduction

Current and emerging generations of radio access technologies such as 5G and Wi-Fi increasingly depend on high-dimensional Channel State Information (CSI) for their operation. Although it is clear that numerous powerful statistical and learning methods could leverage the information geometry contained in CSI distributions, these approaches are hindered by the fact that the high dimension and high sampling rate of CSI makes its storage and further algorithmic processing by resource-constrained baseband processing systems impractical. A pioneering approach to alleviate this issue is channel charting (CC) [1]. It leverages the latent physical and geometrical information embedded in the CSI to extract a lower-dimensional representation, which is easier to exploit. CC can be seen as a building box for a number of applications ranging from radio resource and beam management to geofencing and digital twins [2], with a primary use case being the improvement of location-based applications.

CC methods typically involve two main steps: CSI feature extraction and the subsequent dimensionality reduction (DR) of the obtained features. While the first CC methods focused on non-parametric DR techniques such as Sammon's mapping and principal component analysis (PCA) [1], parametric approaches such as fully-connected (FC) auto-encoders [1], [3], siamese [4], [5] and triplet [6] architectures were also considered, for their ability to easily handle the out-of-sample problem.

This work was supported by ANR (grant no. ANR-23-CHR4-0001-01) under the CHIST-ERA project CHASER (CHIST-ERA-22-WAI-01), and by Horizon Europe SNS project INSTINCT (grant no. 101139161).

Different works have tried to harness the information from different base stations (BS) to enhance the quality of CC [7], [8], [9], [10]. In these works however, although the dataset is distributed, the objective is to train a single model. To our knowledge, only one work [11] has attempted to work with multi-site radio channel maps by extracting separate maps for different BS in a federated manner; in this set-up however, all models operate on the same task. Conversely, in the present paper, *we consider multiple channel charting tasks, with linked tasks* due to the partial overlap between the respective BS coverage areas. This scenario arises when a mobile terminal may communicate with multiple BSs; as a result, the terminal may have a pseudo position in the respective charts of several BSs. Intuitively, this means that the resulting channel charts should also partially overlap. In this scenario, it is necessary to align the latent spaces of the different BSs and to construct an unified channel chart.

This task can be performed through manifold alignment (MA), which seeks to establish relationships between different datasets, with the ultimate goal of projecting samples into a shared embedding space. Supervised (with known sample correspondance) [12] and unsupervised versions of MA [13] have been proposed based on matching the respective manifold Laplacians. [14] proposed to perform MA through a Wasserstein-Procrustes formulation. Optimal transport (OT) can perform MA when a model or function is trained to convert one distribution into another, as implicitly done in [15], [16] in the multi-modality case.

Our main contribution consists in a novel MA-based framework for multi-point channel charting, with the aim of aligning the charts of different BSs, thus facilitating the process of multi-site wireless channel charting. Specifically, we use OT to align each individual channel chart with respect to a geometrical map for each BS, enabling a direct combination of the BSs charts to create an unified chart.

The rest of the paper is structured as follows. Section II details the proposed approach for multi-site CC through latent space alignment. Section III outlines our experimental setup, while in Section IV we present and discuss the results of our experimental validation. Finally, in Section V we conclude and present the guidelines for our future work.

II. Proposed method

We now introduce the considered multi-site CC scenario. For the sake of simplicity, we consider a set-up with two BS,

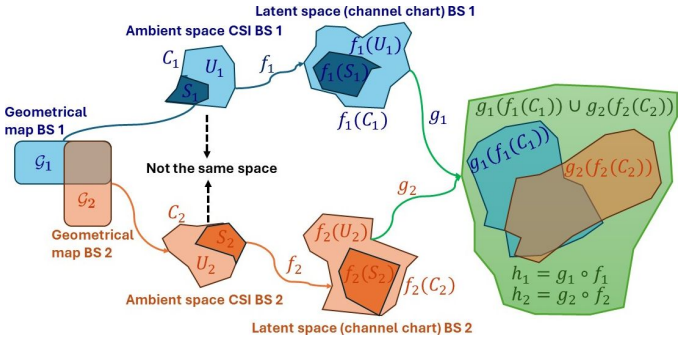

Fig. 1: Problem summary: Two base stations BS_1 and BS_2, with overlapping geometric coverage maps $\mathcal{G}_1$ and $\mathcal{G}_2$, and ambient CSI spaces $\mathcal{C}_1$ and $\mathcal{C}_2$, respectively. Ambient spaces are divided into subsets containing samples from geometric positions shared by both stations ($\mathcal{S}_1$ and $\mathcal{S}_2$), and those containing samples unique to each base station ($\mathcal{U}_1$ and $\mathcal{U}_2$). $\mathcal{C}_1$ and $\mathcal{C}_2$ undergo separate DR through functions f_1 and f_2, yielding CCs $f_1(\mathcal{C}_1)$ and $f_2(\mathcal{C}_2)$. MA is performed through transformations g_1 and g_2 which are applied to the respective CCs, yielding a final CC for each base station, embedded in a common unified channel chart $g_1(f_1(\mathcal{C}_1)) \cup g_2(f_2(\mathcal{C}_2))$.

depicted in Fig. 1; this can be straightforwardly generalized to an arbitrary number of sites. Let $\mathcal{G}_1 \subset \mathbb{R}^2$ and $\mathcal{G}_2 \subset \mathbb{R}^2$ denote the respective geometrical coverage maps of the two base stations BS_1 and BS_2, such that $\mathcal{G}_1 \cap \mathcal{G}_2 \neq \emptyset$. We denote as $\mathcal{C}_i \subset \mathbb{R}^{m_i}$ the CSI acquisition ambient spaces of BS_i. Note that $\mathcal{C}_1$ and $\mathcal{C}_2$ are not embedded in a common space (and in general, $m_1 \neq m_2$); this accounts for the case where BS_1 and BS_2 operate on different bands (e.g. sub-6GHz massive MIMO and mmWave).

For all $i \in \{1,2\}$, denote as $\mathcal{S}_i = \{\mathbf{x} \in \mathcal{C}_i / \mathbf{p_x} \in \mathcal{G}_1 \cap \mathcal{G}_2\}$ the CSI from BS_i that are in the shared area $\mathcal{G}_1 \cap \mathcal{G}_2$ where $\mathbf{p_x}$ is the position of sample $\mathbf{x}$. At last, for all $i \in \{1,2\}$, denote as $\mathcal{U}_i = \mathcal{C}_i \setminus \mathcal{S}_i$ the CSI from BS_i that are not in the shared area, and $\mathcal{P} = \{(\mathbf{u},\mathbf{v}) \in \mathcal{S}_1 \times \mathcal{S}_2 / t_u = t_v\}$ the set of CSI from the different BS generated by the same user at the same moment $t_u = t_v$. Our goal is to learn a CC function for each base station such that $\forall (u,v) \in \mathcal{P}, h_1(u) = h_2(v)$, where $h_i : \mathbb{R}^{m_i} \to \mathbb{R}^2$ is the CC function of BS_i. In the next section, we detail how OT can be used to achieve this goal.

A. Optimal Transport Preliminaries

The main idea of OT is to optimize a transportation plan $\mathbf{T}$ which transports the mass from one source distribution σ to a target distribution τ while minimizing the overall transportation cost. For simplicity, while Fig. 1 illustrates continuous distributions, the rest of the exposition focuses on discrete distributions; CSI sample distributions are naturally discrete, while geographical position distribution can be approximated by discrete distributions since they have low dimension.

In the discrete case, we represent each distribution based on the source and target input data $\mathcal{X} = \{x_1, ..., x_N\}$ and $\mathcal{Y} = \{y_1, ..., y_M\}$, and their weights or masses $\mathbf{s} = [s_1, ..., s_N]^T \in [0,1]^N$ and $\mathbf{t} = [t_1, ..., t_M]^T \in [0,1]^M$:

$$\sigma = \sum_{i=1}^{N} s_i \cdot \delta_{x_i} \quad (1) \qquad \tau = \sum_{j=1}^{M} t_i \cdot \delta_{y_i} \quad (2)$$

where δ_a is the Dirac function at point a, and $\sum_{i=1}^{N} s_i = 1$ and $\sum_{j=1}^{M} t_i = 1$.

A common approach to perform OT is to solve the following regularized optimization problem:

$$\mathcal{L}_{OT}(\mathbf{D},\mathbf{s},\mathbf{t}) = \min_{\mathbf{T} \in \mathbf{U}(\mathbf{s},\mathbf{t})} < \mathbf{T}, \mathbf{D} >_F + \epsilon \cdot H(\mathbf{T}) \quad (3)$$

where $< \cdot, \cdot >_F$ is the Frobenius inner product, $\mathbf{D} \in \mathbb{R}_+^{N \times M}$ is a distance matrix where the element D_{ij} corresponds to the distance between sample $x_i \in \mathcal{X}$ and sample $y_j \in \mathcal{Y}$, ϵ is a hyper-parameter, H is the entropy, and $\mathbf{U}(\mathbf{s},\mathbf{t}) = \left\{\mathbf{T} \in \mathbb{R}_+^{N \times M} | \mathbf{T} \cdot \mathbb{1}_M = \mathbf{s}, \mathbf{T}^T \cdot \mathbb{1}_N = \mathbf{t}\right\}$ for mass preservation. Thanks to the entropic regularization, (3) can be efficiently solved using the Sinkhorn algorithm [17]. For the rest of the paper we assume $\mathbf{s}$ and $\mathbf{t}$ uniform ($s_i = \frac{1}{N}, t_i = \frac{1}{M}\ \forall i$), and denote $\mathcal{L}_{OT}(\mathbf{D},\mathbf{s},\mathbf{t}) = \mathcal{L}_{OT}(\mathbf{D})$.

B. Latent space alignment

This section presents different MA approaches for latent space alignment. They differ mainly in the type of information they use. Note that although the following formulations are based on triplet network architectures, our approach is versatile and not constrained by it.

1) No alignment: This approach consists of training h_1 and h_2 independently, using $\mathcal{C}_1$ and $\mathcal{C}_2$, respectively. For $i \in \{1,2\}$, h_i is given by $\arg\min_h \mathcal{L}_T(h;\mathcal{C}_i)$ where $i \in \{1,2\}$, $\mathcal{L}_T(h,\mathcal{C}_i) = \sum_{x,x_p,x_n \in \mathcal{C}_i} \mathcal{L}_T(x,x_p,x_n;h)$ with $\mathcal{L}_T$ is the triplet loss function depending on an input sample x, two associated positive and negative samples x_p and x_n, and a function h. $\mathcal{L}_T$ is defined as follows:

$$\begin{aligned}\mathcal{L}_T(x,x_p,x_n;h) = \max(0, ||h(x) - h(x_p)||_2 \\ -||h(x) - h(x_n)||_2 + M)\end{aligned} \quad (4)$$

where M is a margin hyper-parameter. As commonly done in CC, we choose the positive and negative samples based on their temporal proximity to the reference sample [6]: positive if the temporal proximity is smaller than $T_c = 5$ s, and negative if it is above T_c.

2) Cell alignment: This approach consists of training h_1 and h_2 independently, using $\mathcal{C}_1$ and $\mathcal{C}_2$. For all $i \in \{1,2\}$ we decompose h_i into $h_i = g_i \circ f_i$, where $f_i : \mathbb{R}^{m_i} \to \mathbb{R}^2$ is a function allowing to obtain a preliminary CC, and $g_i : \mathbb{R}^2 \to \mathbb{R}^2$ is a transformation model aligning the preliminary CC to $\mathcal{G}_i$ and defined for all $\mathbf{x} \in \mathbb{R}^2, g_i(\mathbf{x}) = (\mathbf{M_i x} + \mathbf{b_i}) \oslash \mathbf{a_i}$ with $\mathbf{M_i} \in \mathbb{R}^{2\times2}$, $\mathbf{b_i} \in \mathbb{R}^2$ and $\mathbf{a_i} \in \mathbb{R}^2$ being learnable parameters. We have for all $i \in \{1,2\}$:

$$f_i, g_i = \arg\min_{f,g} \alpha_i \cdot \mathcal{L}_T(f;\mathcal{C}_i) + \beta_i \cdot \mathcal{L}_{OT}^{Cell}(g,f) \quad (5)$$

This function corresponds to an affine transformation. Although it is possible to include the $\mathbf{a_i}$ term within $\mathbf{M_i}$ and $\mathbf{b_i}$, the over-parameterized formulation used here is more amenable to gradient-based optimization and enhances the robustness of the method.

where α_i and β_i are a hyperparameters for the triplet and OT loss functions for BS_i, $\mathcal{L}_{OT}^{Cell}(g, f) = \mathcal{L}_{OT}(\mathbf{D}(\mathcal{C}_i, \mathcal{G}_i; f, g))$ and $\mathbf{D}(\mathcal{C}_i, \mathcal{G}_i; f, g)$ is a distance matrix where for all $i \in \{1, 2\}$, $k \in [1, |\mathcal{C}_i|]$, $l \in [1, |\mathcal{G}_i|]$:

$$\mathbf{D}(\mathcal{C}_i, \mathcal{G}_i; f, g)_{kl} = \frac{1}{2} \cdot ||g(f((\mathcal{C}_i)_k)) - (\mathcal{G}_i)_l||_2^2$$

3) Cell alignment with independent OT: We can also perform the previous implicit alignment in two sequential steps for each BS (with $\alpha_i = 1$ and $\beta_i = 1$), similarly to [16]: first learn the CC function f_i of the BS, then learn the transformation g_i (with a fixed f_i).

4) Cell topology alignment: This approach consists of training $h_1 = g_1 \circ f_1$ and $h_2 : g_2 \circ f_2$ jointly and using one single transform model $g = g_1 = g_2$ to align the CC of both base stations with respect to their geometrical maps:

$$\begin{aligned} f_1, f_2, g = \arg\min_{f_1, f_2, g} \sum_{i=1}^{2} & \alpha_i \cdot \mathcal{L}_T(f_i; \mathcal{C}_i) \\ & + \beta_i \cdot (\mathcal{L}_{OT}(\mathbf{D}(\mathcal{U}_i, \mathcal{G}_i \setminus \mathcal{G}_1 \cap \mathcal{G}_2; f_i, g)) \\ & + \mathcal{L}_{OT}(\mathbf{D}(\mathcal{S}_i, \mathcal{G}_1 \cap \mathcal{G}_2; f_i, g))) \end{aligned} \tag{6}$$

where α_i and β_i are hyperparameters controlling the geometry preservation (triplet loss term), and the alignment (OT loss) for BS_i.

5) Cell topology alignment with independent OT: Similar to *Cell alignment with independent OT*, we can perform this approach in two sequential steps: first learn the CC of each BS through $f_i = \arg\min_f \mathcal{L}_T(f; \mathcal{C}_i)$, then learn the transformations $g_1 = g_2$ for both BS with f_1 and f_2 fixed (with $\alpha_i = 1$ and $\beta_i = 1$):

$$\begin{aligned} g_1 = g_2 = \arg\min_{g} \sum_{i=1}^{2} & \mathcal{L}_{OT}(\mathbf{D}(\mathcal{U}_i, \mathcal{G}_i \setminus \mathcal{G}_1 \cap \mathcal{G}_2; f_i, g) \\ & + \mathcal{L}_{OT}(\mathbf{D}(\mathcal{S}_i, \mathcal{G}_1 \cap \mathcal{G}_2; f_i, g))) \end{aligned} \tag{7}$$

6) Joint Sample and Cell alignment: This approach consists of training h_1 and h_2 jointly and learning one transformation model per BS as in Sec. II-B2 to align the CC of both base stations with respect to their geometrical maps. In addition, to promote proximity among the representations of corresponding samples from different BS in the shared coverage area within the final common CC, we minimize their difference, yielding:

$$\begin{aligned} \arg\min_{f_1, f_2, g_1, g_2} \sum_{i=1}^{2} & \alpha_i \cdot \mathcal{L}_T(f_i; \mathcal{C}_i) + \beta_i \cdot \mathcal{L}_{OT}^{Cell}(g_i, f_i) \\ & + \gamma \cdot \mathcal{L}_{\mathcal{S}_1 \leftrightarrow \mathcal{S}_2}(f_1, g_1, f_2, g_2) \end{aligned} \tag{8}$$

where $\mathcal{L}_{\mathcal{S}_1 \leftrightarrow \mathcal{S}_2}(f_1, g_1, f_2, g_2) = \sum_{(\mathbf{u}, \mathbf{v}) \in \mathcal{P}} ||g_1(f_1(\mathbf{u})) - g_2(f_2(\mathbf{v}))||_2^2$ and α_i, β_i, γ are hyperparameters controlling the geometry preservation (triplet loss term $\mathcal{L}_T$) for BS_i, the alignment (OT loss $\mathcal{L}_{OT}$) for BS_i, and the pairwise correspondence ($\mathcal{L}_{\mathcal{S}_1 \leftrightarrow \mathcal{S}_2}$) respectively.

7) Sample alignment: This method is similar to the previous one, except that we set $\beta_1 = \beta_2 = 0$. As a result, this approach ignores geometric map data and relies solely on associating two samples from different base stations, both generated by the same user at the same location, hence only $\mathcal{P}$ is assumed to be known.

TABLE I: Number of samples per DICHASUS dataset, and per zone. $\mathcal{U}_i$ denotes the unique acquisition zones of BS_i, while $\mathcal{S}_i$ represents the shared coverage areas.

Dataset	$\lvert\mathcal{S}_1\rvert$	$\lvert\mathcal{U}_1\rvert$	$\lvert\mathcal{S}_2\rvert$	$\lvert\mathcal{U}_2\rvert$
cf-02	7 334	6 631	7 334	4 551
cf-03	7 405	11 638	7 405	4 435

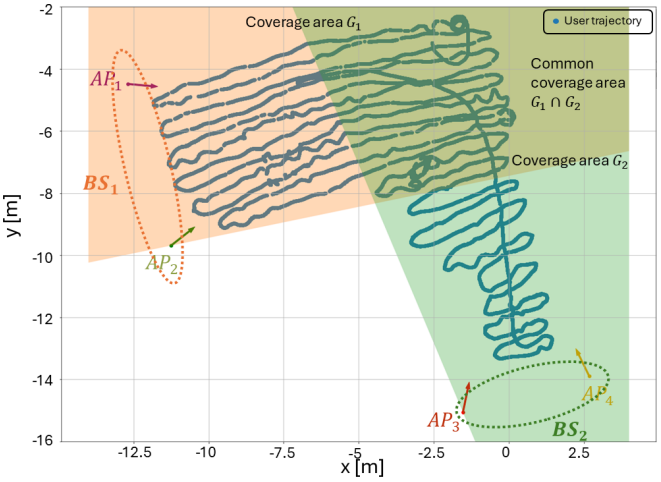

Fig. 2: Indoor DICHASUS dataset split into two virtual base stations, BS_1 and BS_2: BS_1 includes AP_1 and AP_2 (leftmost), and BS_2 includes AP_3 and AP_4 (bottom).

III. Experimental Setup

We evaluate the different methods using DICHASUS [18] datasets: cf-02 for training and cf-03 for testing. These datasets were obtained in an indoor industrial setup. A robot with an omnidirectional antenna moved in an L-shaped area, transmitting pilots to four access points (AP) with 8 antennas each. We create two virtual BSs by combining the two left and the two bottom APs (see Fig. 2). Overlapping coverage is simulated using data masking. The system uses OFDM with 1024 subcarriers over 50 MHz bandwidth at 1.272 GHz center frequency. At last, the data were pre-processed using the pipeline described in [1] and the final count of CSI samples per dataset and BS is detailed in table I.

A. Experiments

We trained a FC network using methods outlined in Sec. II. As a reference, we also trained a centralized single triplet model using all samples for both base stations; we will refer to this model as *Centralized Model*. The NN architecture closely resembles the one from [6], with a slight modification: the number of output features in each FC layer was halved. All the models were trained during 30 epochs with batches of size 1024. Other hyperparameters are indicated in Table II. All experiments were run 5 times, and the results averaged.

Owing to the lack of geometrical coverage information in the dataset, we generated $\mathcal{G}_1$ and $\mathcal{G}_2$ by computing the α-concave hull (with $\alpha = 1$), denoted as $\mathcal{H}_\alpha$, of the ground truth

TABLE II: Hyperparameters used for the different methods. lr corresponds to the learning rate of f_1 and f_2, and $\mathrm{lr_{OT}}$ corresponds to the one of g, g_1, g_2.

Method	lr	$\mathrm{lr_{OT}}$	α_1	α_2	β_1	β_2	γ
Centralized Model	0.05	-	-	-	-	-	
No Alignment	0.1	-	-	-	-	-	-
Cell Alignment	0.1	0.001	1	1	0.001	10	-
Cell Alignment Independent OT	0.1	0.1	1	1	1	1	-
Cell Topology Alignment	0.1	0.01	0.001	0.001	0.01	0.01	-
Cell Topology Alignment Independent OT	0.1	0.01	1	1	1	1	-
Joint Sample and Cell Alignment	0.05	0.05	0.01	0.01	0.1	0.1	0.1
Sample Alignment	0.05	0.05	0.1	0.1	0	0	0.01

(GT) positions of the corresponding samples, followed by the random uniform sampling of 1024 points within the obtained 1-concave hull. Note that while the ground truth positions were used to generate the geometrical coverage maps, they are not used during the training process.

B. Evaluation metrics

1) Alignment metrics: We propose to use different metrics to evaluate CC alignment from both BS. First, if we denote as IoU(A, B) the intersection over union of two polygons A and B, we compute $\mathrm{IoU_C} = \mathrm{IoU}(\mathcal{H}_1(h_1(\mathcal{S}_1)), \mathcal{H}_1(h_2(\mathcal{S}_2)))$ where higher values indicate a better overlap between common coverage areas. We also compute the mean over i of $1-\mathrm{IoU_i} = 1-\mathrm{IoU}(\mathcal{H}_1(h_i(\mathcal{U}_i)), \mathcal{H}_1(h_i(\mathcal{S}_i)))$, and we denote it $1-\mathrm{IoU_{BS}}$, where higher values indicate less overlap between the CC positions of CSI samples that are not acquired by both BS and the ones that are. Second, we propose to use the FOSCTTM metric, introduced in [14], representing the fraction of samples closer than the true match.

2) Dimensionality reduction metrics: We employed trustworthiness (T) and Kruskal Stress (T) to assess the preservation of the local structure of the ambient space. For more details we refer the reader to [6]. For assessing the preservation of the global structure, we employed the order 1 Wasserstein distance (WD).

IV. Results and Discussion

A. Multi-BS alignment

We first focus on assessing the capability of the different studied methods to align channel charts across multiple BSs. The results are detailed in Table III and illustrated in Fig. 3.

Observations reveal that *Cell Topology Alignment* emerges as the most overall effective method for CC alignment: it outperforms other methods significantly with lower variability. Notably, its performance closely resembles that of the *Centralized Model*. The superiority of *Cell Topology Alignment* comes from its explicit alignment of individual and shared coverage areas with associated geometrical maps, unlike other methods. Moreover, its outperformance over *Joint Sample and Cell Topology Alignment* is due to the latter's less refined alignment across entire coverage areas rather than treating them separately. This refinement is critical as uniform weights assumed in the OT problem can lead to mismatches, emphasizing the significance of *Cell Topology Alignment*.

Furthermore, *Joint Sample and Cell Alignment* outperforms *Cell Topology Alignment* in FOSCTTM. Yet, for localization and distance measurement, the discontinuities between BS coverage areas observed for *Joint Sample and Cell Alignment* (Fig. 3) are problematic, unlike with *Cell Topology Alignment* (smooth CC transitions are preferable to avoid abrupt user zone changes). However, the observed enhancement in terms of FOSCTTM with *Joint Sample and Cell Alignment* compared to *Cell Topology Alignment* is noteworthy. In shared coverage areas, each measurement has two representations (one per BS). Thus, it is crucial for these CC coordinates to align closely. The reduced FOSCTTM of *Joint Sample and Cell Alignment* indicates that its aligned CC results in fewer false positives in common areas. This means that for a given point in the shared coverage area in the CC of one BS, there are fewer points from the other BS closer to it than its true corresponding point, compared to other methods.

Finally, despite *No Alignment* obtaining the CC of each BS independently, it still shows noticeable alignment, occasionally outperforming other methods relying on OT or distance minimization. This highlights Channel Charting's inherent capability to map radio environments; shared coverage areas likely have similar propagation environments, leading to similar CC.

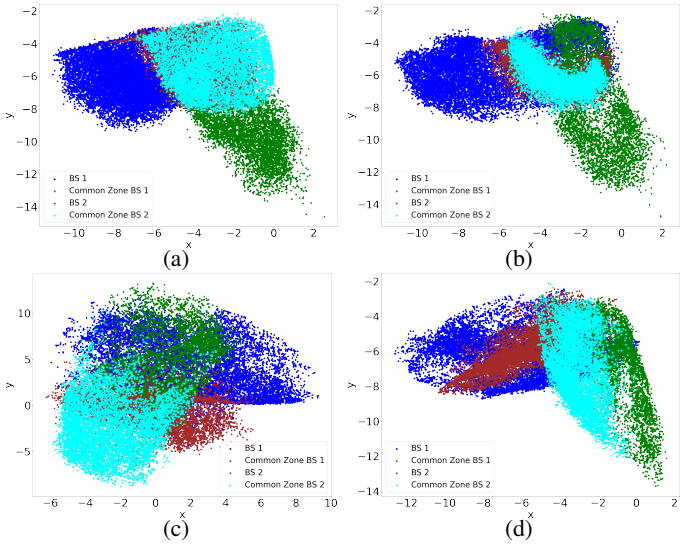

Fig. 3: Combined best final channel charts for the top 4 best performing methods over five repetitions (choice based on $\mathrm{IoU_C}$). (a) Cell Topology Alignment, (b) Joint Sample and Cell Alignment, (c) No Alignment, (d) Cell Alignment with Independent OT.

B. Local and global structure of the charts

We analyze CCs' local/global structure, crucial for certain applications. Results can be found in Table III.

First, we observe that the best overall performing method in terms of local structure preservation is *Cell Topology Alignment*, with improvements of T and KS, often reducing the variability. Its refined alignment process aligns unique coverage zones with each other and common coverage areas

TABLE III: Alignment and dimensionality reduction results of the different compared approaches. Best results in bold, second-best in italic. $\mathcal{S}_1 \leftrightarrow \mathcal{S}_2$ denotes the use of the sample-by-sample correspondence between the elements of $\mathcal{S}_1$ and $\mathcal{S}_2$.

Method	$\mathcal{G}_\mathbf{i}$	$\mathcal{G}_\mathbf{1} \cap \mathcal{G}_\mathbf{2}$	$\mathcal{G}_\mathbf{1} \setminus \mathcal{G}_\mathbf{2}$	$\mathcal{G}_\mathbf{2} \setminus \mathcal{G}_\mathbf{1}$	$\mathcal{S}_1 \leftrightarrow \mathcal{S}_2$	$\mathbf{IoU_C} \uparrow$	$\mathbf{1 - IoU_{BS}} \uparrow$	$\mathbf{FOSCTTM} \downarrow$	$\mathbf{T} \uparrow$	$\mathbf{KS} \downarrow$	$\mathbf{WD} \downarrow$
Centralized Model	×	×	×	×	×	$\mathbf{76.42 \pm 3.97}$	45.97 ± 2.97	$\mathbf{34.15 \pm 1.60}$	72.99 ± 0.85	*0.48 ± 0.01*	5.89 ± 3.12
No Alignment	×	×	×	×	×	29.46 ± 16.49	43.82 ± 2.81	50.25 ± 3.55	*74.81 ± 4.94*	0.54 ± 0.02	5.23 ± 0.45
Cell Alignment	✓	×	×	×	×	28.41 ± 12.30	36.89 ± 3.67	49.74 ± 3.02	72.51 ± 3.24	b0.55 ± 0.07	0.54 ± 0.13
Cell Alignment Independent OT	✓	×	×	×	×	22.18 ± 3.44	44.69 ± 2.36	51.09 ± 1.91	74.10 ± 1.33	0.58 ± 0.05	*0.47 ± 0.07*
Cell Topology Alignment	×	✓	✓	✓	×	*71.76 ± 10.10*	$\mathbf{76.62 \pm 6.05}$	49.68 ± 1.49	$\mathbf{75.27 \pm 1.21}$	$\mathbf{0.46 \pm 0.02}$	$\mathbf{0.28 \pm 0.09}$
Cell Topology Alignment Independent OT	×	✓	✓	✓	×	29.34 ± 12.09	39.76 ± 2.32	48.50 ± 5.62	74.20 ± 2.06	0.53 ± 0.05	0.84 ± 0.34
Joint Sample and Cell Alignment	✓	×	×	×	✓	55.08 ± 14.40	74.16 ± 5.76	*40.23 ± 1.70*	*74.14 ± 1.43*	0.52 ± 0.02	0.986 ± 0.003
Sample Alignment	×	×	×	×	✓	11.62 ± 8.34	60.06 ± 8.32	49.95 ± 0.89	68.11 ± 3.28	0.69 ± 0.03	5.32 ± 0.15

accordingly, for each BS, enhancing T by minimizing the occurrence of distant samples becoming neighbours in the final CC. This also leads to a decrease in KS (distance preservation). Evaluating local structure preservation metrics on the final CC shows that samples from both BS_1 and BS_2 can be neighbors, especially within common coverage areas, further improving local structure preservation compared to individual BS measurements.

Second, it is noteworthy that the *Cell Topology Alignment* model stands out as the best one based on global structure preservation. This superiority can be attributed to two main factors. Firstly, methods that align CCs to geometric maps have an inherent advantage because the Wasserstein Distance is as an OT distance. This alignment to geometric maps has practical benefits, such as enabling real coordinate localisation and proximity detection of users. Secondly, *Cell Topology Alignment* operate on zones instead of aligning each CC with the entire geometric maps of their corresponding BS. This approach effectively brings CC samples closer to their GT positions, despite the uniform weights assumption.

Finally, it is important to note that we did not prioritise hyperparameter optimisation, so there is potential for further advances, especially if optimised individually for each BS.

V. Conclusion

In this work, we introduced a novel framework for multi-point channel charting. Instead of fusing information from different BSs and focusing on a single task, we extract individual CCs for each BS with partially overlapping coverage areas, while aligning these common coverage areas within the CCs. Within this framework, we proposed several methods to align the CCs of different BSs, yielding promising results.

Finally, to further optimise the efficiency of these approaches, it would be beneficial to adapt the methods we have introduced for training and use in a distributed manner. Additionally, although our study focuses on the two BSs scenario, it can be extended to more BSs. In this case, it is important to note that the amount of information shared between BSs increases with their number.

References

[1] C. Studer, S. Medjkouh, E. Gonultaş, T. Goldstein, and O. Tirkkonen, "Channel charting: Locating users within the radio environment using channel state information," *IEEE Access*, vol. 6, 2018.

[2] P. Ferrand, M. Guillaud, C. Studer, and O. Tirkkonen, "Wireless channel charting: Theory, practice, and applications," *IEEE Communications Magazine*, vol. 61, no. 6, pp. 124–130, 2023.

[3] P. Huang, O. Castañeda, E. Gönültaş, S. Medjkouh, O. Tirkkonen, T. Goldstein, and C. Studer, "Improving channel charting with representation -constrained autoencoders," in *IEEE 20th International Workshop on Signal Processing Advances in Wireless Communications*, 2019.

[4] E. Lei, O. Castañeda, O. Tirkkonen, T. Goldstein, and C. Studer, "Siamese neural networks for wireless positioning and channel charting," in *57th Annual Allerton Conference on Communication, Control, and Computing*, 2019, pp. 200–207.

[5] M. Stahlke, G. Yammine, T. Feigl, B. Eskofier, and C. Mutschler, "Indoor Localization with Robust Global Channel Charting: A Time-Distance-Based Approach," *IEEE Transactions on Machine Learning in Communications and Networking*, vol. 1, 2023.

[6] P. Ferrand, A. Decurninge, L. G. Ordoñez, and M. Guillaud, "Triplet-based wireless channel charting: Architecture and experiments," *IEEE Journ. Sel. Areas in Comm.*, vol. 39, no. 8, pp. 2361–2373, 2021.

[7] J. Deng, S. Medjkouh, N. Malm, O. Tirkkonen, and C. Studer, "Multipoint channel charting for wireless networks," in *Proc. Asilomar Conference on Signals, Systems, and Computers*, 2018, pp. 286–290.

[8] T. Ponnada, H. Al-Tous, O. Tirkkonen, and C. Studer, "An out-of-sample extension for wireless multipoint channel charting," in *Proc. International Conference on Cognitive Radio-Oriented Wireless Networks Conference*, Germany, 2019, pp. 208–217.

[9] C. Geng, H. Huang, and J. Langerman, "Multipoint channel charting with multiple-input multiple-output convolutional autoencoder," in *IEEE/ION Position, Location and Navigation Symposium*, 2020, pp. 1022–1028.

[10] J. Pihlajasalo, M. Koivisto, J. Talvitie, S. Ali-Löytty, and M. Valkama, "Absolute positioning with unsupervised multipoint channel charting for 5G networks," in *Proc. IEEE Vehicular Tech. Conference*, Nov. 2020.

[11] P. Agostini, Z. Utkovski, and S. Stańczak, "Federated learning for multipoint channel charting," in *Proc. International Workshop on Signal Processing Advances in Wireless Communication (SPAWC)*, 2022.

[12] C. Wang, P. M. Krafft, and S. Mahadevan, "Manifold alignment," in *Manifold Learning Theory and Applications*, Y. Ma and Y. Fu, Eds. CRC Press, Dec. 2011.

[13] Z. Cui, H. Chang, S. Shan, and X. Chen, "Generalized unsupervised manifold alignment," in *Advances in Neural Information Processing Systems*, vol. 27, 2014.

[14] D. Chen, B. Fan, C. Oliver, and K. Borgwardt, "Unsupervised manifold alignment with joint multidimensional scaling," in *11th International Conference on Learning Representations*, 2023.

[15] F. Ghazvinian Zanjani, I. Karmanov, H. Ackermann, D. Dijkman, S. Merlin, M. Welling, and F. Porikli, "Modality-agnostic topology aware localization," in *Advances in Neural Information Processing Systems*, vol. 34, 2021, pp. 10 457–10 468.

[16] M. Stahlke, Y. George, T. Feigl, B. Eskofier, and C. Mutschler, "Velocity-Based Channel Charting with Spatial Distribution Map Matching," *IEEE Sensors Journal*, p. 8, 2023.

[17] P. A. Knight, "The Sinkhorn–Knopp algorithm: convergence and applications," *SIAM Journal on Matrix Analysis and Applications*, vol. 30, no. 1, pp. 261–275, 2008.

[18] F. Euchner, M. Gauger, S. Dörner, and S. ten Brink, "A Distributed Massive MIMO Channel Sounder for "Big CSI Data"-driven Machine Learning," in *25th International Workshop on Smart Antennas*, 2021.